Taylor & Francis
Taylor & Francis Group

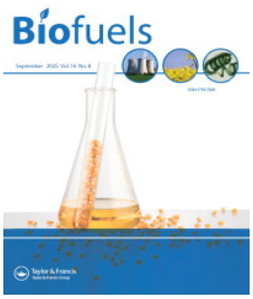

Biofuels

ISSN: 1759-7269 (Print) 1759-7277 (Online) Journal homepage: www.tandfonline.com/journals/tbfu20

Cork waste-based adsorbents for glycerol removal from biodiesel: a sustainable alternative to wet washing

Maria Isabella Lima Garção, Eduardo Candido Milani, Gabriel Lamino Camilo, Jose L. Diaz De Tuesta, Maria Carolina Sérgi Gomes, António E. Ribeiro, Ana Queiroz & Paulo Brito

To cite this article: Maria Isabella Lima Garção, Eduardo Candido Milani, Gabriel Lamino Camilo, Jose L. Diaz De Tuesta, Maria Carolina Sérgi Gomes, António E. Ribeiro, Ana Queiroz & Paulo Brito (14 Jun 2025): Cork waste-based adsorbents for glycerol removal from biodiesel: a sustainable alternative to wet washing, Biofuels, DOI: 10.1080/17597269.2025.2517453

To link to this article: https://doi.org/10.1080/17597269.2025.2517453

BIOFUELS
https://doi.org/10.1080/17597269.2025.2517453

Taylor & Francis
Taylor & Francis Group

Cork waste-based adsorbents for glycerol removal from biodiesel: a sustainable alternative to wet washing

Maria Isabella Lima Garção[a,b,c], Eduardo Candido Milani[a,b,c], Gabriel Lamino Camilo[a,b,c], Jose L. Diaz De Tuesta[d], Maria Carolina Sérgi Gomes[c], António E. Ribeiro[a,b], Ana Queiroz[a,b] and Paulo Brito[a,b]

[a]Centro de Investigação de Montanha (CIMO), Instituto Politécnico de Bragança, Bragança, Portugal; [b]Laboratório Associado para a Sustentabilidade e Tecnologia em Regiões de Montanha (SusTEC), Instituto Politécnico de Bragança, Bragança, Portugal; [c]Postgraduate Program in Chemical Engineering, Federal University of Technology of Parana –Universidade Tecnológica Federal do Paraná, Apucarana, Brasil; [d]Chemical and Environmental Engineering Group, ESCET, Rey Juan Carlos University, Móstoles, Spain

ABSTRACT

This work aims to use activated carbon from industrial cork waste as a novel method for glycerol removal from crude biodiesel produced using waste cooking oil, combining two residues to obtain both high-quality biodiesel and highly adsorbent activated carbon. The study first optimizes the biodiesel production conditions, achieving the highest ester yield at 30 °C, with a 1:9 oil-to-ethanol molar ratio, 1 wt.% NaOH catalyst, and a reaction time of 1 h. Additionally, activated carbons were prepared and characterized from cork waste, showing significantly higher BET surface areas than the raw material. The most promising cork-based materials were then applied to optimize glycerol removal from crude biodiesel through adsorption. A preliminary study identified milled raw cork and its KOH-activated carbon (SBET = 2057 m^2/g) as the most effective. Kinetic and equilibrium studies demonstrated that optimal glycerol removal was achieved after 6 h at 25 °C using 2 wt.% of KOH-activated cork-based adsorbent, resulting in 88% glycerol removal and a final glycerol content of 0.017 wt.%. These findings demonstrate that cork waste-derived activated carbon is highly effective for biodiesel purification, successfully meeting the quality specifications required by European Standard EN 14214:2012+A2:2019 and offering an innovative solution for waste valorization and sustainable fuel production.

ARTICLE HISTORY
Received 13 February 2025
Accepted 5 June 2025

KEYWORDS
Biodiesel purification; glycerol removal; adsorption equilibrium; adsorption kinetics; activated carbon

Introduction

Global energy consumption has risen over the past few decades, and the International Energy Agency predicts that the energy demand will increase by 50% by 2030 [1]. This surge in demand, coupled with the limited supply of fossil fuels and the environmental problems associated with their use, has led researchers to explore alternative energy sources. Among these alternatives, biofuels have emerged as a promising option, and biodiesel, in particular, has gained much attention [2].

Biodiesel is a renewable energy source produced from various resources, including waste cooking oil (WCO), oily sludge from factories, and discarded animal fats [3]. Compared to petroleum-derived diesel, biodiesel has lower carbon emissions and is more environmentally friendly. It is renewable, biodegradable, non-toxic, sulfur-free, and aromatic carcinogen-free. While biodiesel costs are currently higher than petroleum diesel, using WCO as a feedstock can reduce the cost significantly, since it is 25% to 40% of the edible oil price [4].

The most common method for producing biodiesel is through the transesterification reaction, which converts oils or free fatty acids into alkyl esters and glycerol [5]. The properties of biodiesel depend on the feedstock used, and it must meet specific standards, such as the European Standard EN 14214:2012+A2:2019 [6]. This standard defines characteristics that determine the behavior of biodiesel combustion in an engine and the methods used to determine those parameters. To meet these specifications, the biodiesel produced must be purified to remove impurities such as glycerol, which must be no more than 0.02 wt.%.

There are two standard methods of purifying biodiesel: wet and dry washing. More traditional wet washing methods are often used to remove excess contaminants and other remaining products from biodiesel. In this method, for every liter of biodiesel,

CONTACT Maria Isabella Lima Garção m.limagarcao@gmail.com Instituto Politécnico de Bragança, Campus de Santa Apolónia, 5300-253 Bragança, Portugal; Jose L. Diaz De Tuesta joseluis.diaz@urjc.es Chemical and Environmental Engineering Group, ESCET, Rey Juan Carlos University, C/Túlipan, s/n, 28933, Móstoles, Spain.

almost 10 L of wastewater is produced [7,8]. However, adding additional water to the process has several disadvantages, including generating a high amount of chemically unsuitable effluent for discharge into any body of water, increased cost, and production time. Additionally, wet washing allows emulsions that prevent the esters from separating and the formation of free acids and soap [9].

Dry-washing processes use adsorbents or ion exchange resins to purify biodiesel. These processes rely on filtration, physical adsorption, or ion exchange. It offers several advantages, such as better fuel quality, easier process integration, and shorter operation time [10]. Compared to wet washing, dry-washing processes are more efficient and cost-effective. They produce higher-quality biodiesel, require less time to operate, and do not generate any wastewater, making them a more environmentally friendly option [11].

Several studies have been conducted on biodiesel purification by adsorption. Materials like magnesol and rice husk ash [12], oil palm empty fruit brunch [13], and modified commercial adsorbents [14] have shown promising outcomes in biodiesel purification. They have acidic or basic adsorption sites with a strong affinity with polar compounds such as ethanol, glycerol, metals, and soap [15].

Recent studies of biodiesel purification through adsorption utilize biodiesel characterized by a low glycerin concentration, such as 0.0301 and 0.064 wt.% in the works of Alves et al. and Paschoal et al. respectively [11,16]. However, a notable gap exists in studies addressing biodiesel produced from WCO, characterized by significantly higher glycerin content and increased impurities. This knowledge disparity underscores the need for adsorbents with enhanced adsorption capacities to remove these impurities efficiently, meeting the stringent requirements outlined in the European Standard EN 14214:2012+A2:2019 [6].

Alves et al. [11] studied biodiesel purification through adsorption using sugarcane bagasse as an adsorbent and showed that this method can purify the produced ester according to the standard requirements. Sandouqa et al. [17] also studied the purification step and removed all glycerol from biodiesel using olive cake residues as adsorbent.

Cork is an environmentally friendly and renewable resource that has been increasingly used as an adsorbent in recent years. Its high porosity and specific surface area make it an effective material for removing pollutants from water and air [18]. The unique porous structure of cork has received the attention of researchers in various fields, including its potential as an adsorbent for pollutants such as heavy metals, organic compounds, and dyes. In addition to the effectiveness of the cork, its low cost, biodegradability, and ease of regeneration make it an attractive alternative to traditional adsorbents [19]. Additionally, Portugal leads the globe in cork production, supplying about 100,000 tonnes annually, accounting for 55% of the worldwide output [20]. Ongoing research is focused on optimizing cork adsorption capacity and performance. The homogeneous porous structure of cork has also made it a valuable material for activated carbon (AC) synthesis. Its ability to maintain structure under high-temperature conditions creates numerous diffusion channels and a high surface area, which is advantageous in adsorption [18,21,22]. Furthermore, bio-based carbon materials possess expansive surface areas, diverse structures, and customizable properties, all at an affordable cost. Additionally, the abundance of available bio-based waste presents a significant opportunity for achieving sustainability in material utilization [23].

This study investigates the viability of cork and cork-derived activated carbons for biodiesel purification, filling a gap in existing literature. Leveraging the abundance of cork waste in Portugal, it proposes dry washing as an alternative to conventional methods, analyzing adsorption kinetics and isotherms. A detailed description of the dry-washing methodology can be found in a previous review paper [24]. The purposes of the present work were: (1) to optimize biodiesel production, (2) to study the production and characterization of activated carbons from cork waste, and (3) to select and optimize the most effective cork waste-based adsorbent for glycerol removal from biodiesel.

Materials and experimental methods

Waste cooking oil characterization

The fatty acid profile of WCO was analyzed using a Shimadzu Nexis GC-2030 gas chromatography system equipped with an FID detector, an IOC-20i automatic injection system, and an OPTIMA® BioDiesel F capillary column. The sample preparation involved dissolving 25 mg of WCO in a KOH (+88.5%, Pronlab) solution, heating it at 90 °C, cooling it, and then adding BF_3 (Sigma Aldrich) in methanol (+99.8%, Fischer Scientific) before reheating. After cooling again, an internal standard solution was added, followed by a saturated sodium chloride (+99%, Panreac) solution. The mixture was stirred and centrifuged at 3000 rpm for 5 min. The upper phase was collected, dried with anhydrous sodium sulfate (Carlo Erba), and analyzed by gas chromatography.

Biodiesel production by transesterification

Biodiesel was produced *via* transesterification using WCO and ethanol (+99%, Carlo Erba) as feedstock, with NaOH (+98%, Honeywell) as the catalyst. The process was tested at 30 °C, 45 °C, and 60 °C, with oil-to-alcohol molar ratios of 1:6, 1:7.5, and 1:9 to maximize fatty acid ethyl ester's (FAEEs) yield. Catalyst loading was fixed at 1 wt.% of the oil mass, as recommended by Oraegbunam et al. [25].

The reaction lasted 1 h, after which excess ethanol was removed using a rotary evaporator (150 mbar, 45 °C for 0.5 h). Lastly, decantation separated the lighter phase (biodiesel) from the heavier phase - glycerol and other impurities. The FAEEs yield of biodiesel was measured through gas chromatography following the European Standard EN 14103:2020 [26].

Activated carbon production and characterization

The adsorbents were produced through a two-step carbonization of milled raw cork waste (Amorim Cork Composites Industry) with KOH activation. Four types of activated carbon were prepared following Wang et al. [19]. First, 4 g of milled cork was carbonized in a muffle furnace (Thermolyne 6000, 550 °C, 1 or 2 h, 10 °C/min heating rate), producing CC1 and CC2, respectively. Next, CC1 and CC2 were mixed with KOH in a 1:5 (CC:KOH) weight ratio and subjected to a second carbonization at 750 °C for 2 h, yielding CCB1 and CCB2. The final products were washed with 0.1 M HCl (+37%, Honeywell) and distilled water to neutral pH, then dried overnight at 100 °C. A preparation flowchart is available in the supplementary material.

All prepared materials were characterized by the experimental determination of the surface area, elemental composition, pH at point of zero charge (pH_{PZC}), spectrophotometric analysis using FT-IR, and thermogravimetric analysis (TGA).

The N_2 adsorption-desorption measurements needed to quantify the surface area were performed at 77 K using Quantachrome NOVATOUCH LX^2. Before the experiments, all materials were degassed at 120 °C for 6 h. The surface area was calculated using the BET (Brunauer, Emmett, and Teller) model and *t*-plot method to determine micropore surface area.

Elemental composition was determined using a CHNS analyzer (Flash 2000, Thermo Fisher Scientific) with a thermal conductivity detector, operating in an oxidation/reduction reactor at 900 °C. The pH_{PZC} of the prepared materials was evaluated according to Rovani [27]. The pH_{PZC} was determined by identifying where ΔpH vs. pHi intersects with the x-axis ($y = 0$). FTIR spectroscopy was conducted using a Perkin Elmer Spectrum Two instrument, analyzing wavenumbers between 400 and 4000 cm^{-1} with KBr-prepared tablet samples. Thermogravimetric analysis (TGA) was performed using a simultaneous TGA-DSC thermobalance (TGA-DCS1100, Mettler-Toledo) from 40 °C to 900 °C under nitrogen at a heating rate of 10 °C min^{-1}. Proximate analysis was conducted to determine moisture, volatile matter, ash, and fixed carbon content. Moisture and volatile matter were measured as weight loss up to 105 °C and 900 °C in an inert atmosphere, while ash content was calculated as the remaining weight at 900 °C in an oxidizing atmosphere. Fixed carbon was determined by subtracting the percentages of moisture, volatile matter, and ash from 100%.

Adsorption experiments

A preliminary adsorption experiment was conducted to identify the most effective adsorbent for glycerol removal. Five materials—milled raw cork, CC1, CC2, CCB1, and CCB2—were tested in a shaker incubator (25 °C, 150 rpm, 8 h) with 2.5 wt.% adsorbent loads. For the quantification of free glycerol, the detection methodology through UV-vis, described by Bondioli and Della Bella [28] was used, which consists of a two-step reaction that generates a yellow complex proportional to the amount of free glycerol and has a maximum absorbance at 410 nm.

Adsorption capacity and removal efficiency were calculated using Equation (3) and Equation (4), based on glycerol concentration changes in biodiesel and adsorbent load, where q is the amount of adsorbed glycerol per gram of adsorbent ($mg_{adsorbate}/g_{adsorbent}$), C_i and C_f is the adsorbate initial and final concentration at the equilibrium ($mg.g^{-1}$), m_b and m_a is the mass of biodiesel and adsorbent (g), respectively, and R is the removal efficiency (%).

$$q = \frac{(C_i - C_f) \times m_b}{m_a} \tag{1}$$

$$R(\%) = \frac{(C_i - C_f)}{C_i} \times 100 \tag{2}$$

The kinetics of the adsorption process for the materials were studied at three different temperatures (25, 35, and 45 °C) using adsorbent loads of 2 and 3 wt.%. The experiments used a magnetic stir plate (MultiMix D MM90E) at 300 rpm. Samples of 1 mL were taken at intervals ranging from 5 to 1440 min for analysis and then filtered using a syringe filter to have their glycerol content analyzed.

The equilibrium adsorption isotherms were experimentally measured through the batch method, using a magnetic stirring plate (MultiMix DMM90E at

300 rpm) for 25, 35, and 45 °C, and adsorbent concentrations from 0.1 to 3 wt.%.

All adsorption experiments – preliminary, kinetics, and equilibrium – were conducted in triplicate.

Adsorption kinetics and equilibrium models

The pseudo-first order (PFO, Equation (5)), pseudo-second order (PSO, Equation (6)), Elovich model (Equation (7)), and the intraparticle diffusion model proposed by Weber and Morris (Equation (8)) (PFO, Equation (3)), pseudo second order (PSO, Equation (4)), Elovich model (Equation (5)), and the intraparticle diffusion model proposed by Weber and Morris (Equation (6)) were fitted to the experimental kinetic data.

$$q_t = q_e(1 - e^{-k_1 t}) \tag{3}$$

$$q_t = \frac{q_e^2 k_2 t}{k_2 q_e t + 1} \tag{4}$$

$$q_t = \frac{1}{\beta}\ln(1 + \alpha\beta t) \tag{5}$$

$$q_t = k_{id}\sqrt{t} + C \tag{6}$$

In all equations, q_t and q_e are the amount of glycerol adsorbed in the solid ($mg_{adsorbate}/g_{adsorbent}$) at the time t and at the equilibrium, respectively. The parameters k_1 (min^{-1}) and k_2 ($g_{adsorbent}/(mg_{adsorbate}\,.\,min)$ are the adsorption rate constants. α and β are the initial adsorption rate ($mg_{adsorbate}/(g_{adsorbent}.min)$ and the desorption parameter ($g_{adsorbent}/mg_{adsorbate}$), respectively. Lastly, k_{id} represents the intraparticle diffusion rate ($mg_{adsorbate}/(g_{adsorbent}\,.\,min^{0.5})$, and C is the Weber and Morris model constant ($mg_{adsorbate}/g_{adsorbent}$).

The equilibrium adsorption models were fitted to the experimental data to understand adsorption behavior better. The selected models are the Freundlich, Radke-Prausnitz, and Sips models (See Equations (7)–(9), respectively).

$$q_e = K_F C_e^{n_F^{-1}} \tag{7}$$

$$q_e = \frac{ABC_e^{\beta}}{A + BC_e^{(\beta-1)}} \tag{8}$$

$$q_e = \frac{Q_S K_S C_e^{n_S}}{1 + K_S C_e^{n_S}} \tag{9}$$

K_F and n_F^{-1} represent the Freundlich isotherm constant ($g_{biodiesel}/g_{adsorbent}$) and the heterogeneity factor (-), respectively. In the Radke-Prausnitz model, A ($g_{biodiesel}/g_{adsorbent}$) and B [$(mg_{adsorbate}/g_{adsorbent})/(mg_{adsorbate}/mg_{adsorbate})^{\beta}$] are the constants, and the exponent β varies between 0 and 1. The Sips model (Equation (11)) is a combination of Freundlich and Langmuir isotherm models [29]. The Q_S ($mg_{adsorbate}/g_{adsorbent}$) is the maximum adsorption capacity, K_S ($g_{biodiesel}/mg_{adsorbate}$) and n_S (-) is the model exponent.

Although the Langmuir and Toth isotherms are commonly used in adsorption studies, they were not applied here due to their assumption of homogeneous adsorption sites. Given the complex and heterogeneous nature of the biodiesel matrix, these models were considered unsuitable for accurately representing the adsorption data.

Further explanation on the kinetic and equilibrium models can be found in the supplementary material.

Models fitting and evaluation

A standard approach to estimating adsorption kinetics and equilibrium isotherm parameters involves linearizing nonlinear equations, as seen with the previously presented models. However, Guo and Wang [30] showed that linearization can introduce propagated errors, leading to biased and inefficient parameter estimates. To avoid this, the authors directly fitted the models to experimental data, selecting the model that minimizes an error function, with the mathematical expression for this error function described in Equation (10), adapted from Baysal et al. [31]. N is the number of experimental points, p is the number of estimated parameters, q_{exp} is the experimental concentration in the adsorbent and q_{cal} is the concentration in the adsorbent predicted by the selected model. Additionally, Equation (11) was used to estimate the correspondent reduced Qui-Square statistic function.

$$\Delta q(\%) = 100\sqrt{\frac{1}{n-p}\sum\left[\frac{(q_{exp} - q_{cal})}{q_{exp}}\right]^2} \tag{10}$$

$$Red\ \chi^2 = \frac{1}{n-p}\sum\left[\frac{(q_{exp} - q_{cal})^2}{q_{exp}}\right] \tag{11}$$

Results and discussion

Waste cooking oil derivatization

The GC-FID analysis of the WCO after derivatization was made in triplicate. Table 1 presents the results of the percentage of each fatty acid present in the derivatized WCO sample. The analysis showed that the esters present in higher concentrations were

Table 1. Fatty acids composition in the WCO sample in terms of lipid number and fatty acid methyl ester (FAME) content.

Fatty acid	Lipid number	FAMEs (wt.%)
Palmitic acid	C16:0	8.21 ± 0.06
Stearic acid	C18:0	3.24 ± 0.02
Oleic acid, Elaidic acid	C18:1	28.53 ± 0.42
Linoleic acid, Linonaidic acid	C18:2	44.36 ± 0.16
alpha-Linolenic acid	C18:3	1.87 ± 0.01
Total		86.38 ± 0.38

palmitic acid (C16:0), stearic acid (C18:0), oleic acid (C18:1), linoleic acid (C18:2), and alpha-linolenic acid (C18:3).

The analysis of the WCO composition shows that the sample is rich in unsaturated fatty acids, particularly C18:1 and C18:2, which account for more than 72% of the total fatty acids. An increase in the degree of unsaturation leads to a decrease in the oxidative stability, heat of combustion, and cetane number, as well as the melting and boiling points of the oil [32]. However, a higher ratio of unsaturated to saturated fatty acids results in a lower fusion point and greater fluidity, crucial parameters for viscosity and crystallization, providing good fuel performance at low temperatures [32,33]. Therefore, WCO, with its high content of unsaturated fatty acids, is highly suitable for producing biodiesel due to its favorable fluidity characteristics.

Biodiesel production and characterization

Following the transesterification reaction and phase separation, the yield of FAEEs in the biodiesel phase was analyzed using gas chromatography, as previously described. The yield results are shown in Figure 1.

For all operation conditions that led to phase separation, the ester yield was greater than 76%. However, when the proportion of oil to alcohol was 1:6, the temperature of 30 °C represented a barrier to phase separation, and a competition between the saponification and the transesterification reactions was observed. The same competition was observed at a ratio of 1:7.5, but to a lesser extent, as two phases were formed for 30 and 45 °C. At this proportion, an increase in temperature did not favor the formation of esters, and the FAEE's yield decreased from 83.76 ± 1.19% to 76.40 ± 0.86%. When the excess of alcohol was increased to a molar ratio of 1:9, the effect of saponification was overcome, and two phases were formed at all temperatures. However, the yield of esters continued to decrease with an increase in temperature, falling from 88.26 ± 0.17% at 30 °C to 81.00 ± 0.12% at 60 °C.

The highest yield of FAEEs was obtained at 30 °C and a 1:9 oil:alcohol molar ratio, consistent with previous research. For instance, Silva et al. [34] conducted a factorial design for ethyl biodiesel production. They concluded that lower temperatures increase the yield of FAEE when the molar proportion of oil:alcohol is below 1:10. This finding was also supported by Gomes [33], who found that the yield was higher at temperatures below 40 °C and a molar proportion higher than 1:7.5. The study also reported that at higher temperatures, parallel reactions such as saponification were favored, leading to a decrease in the yield of FAEE.

Cork-based activated carbon characterization

The textural properties obtained for activated carbon are shown in Table 2, where S_{BET} is the BET surface area, S_{mic} is the micropore area, V_t is total pore volume, V_{mic} is micropore volume, and D_p is the average pore diameter.

The use of KOH in activated carbon production yields materials with a broad range of attributes, such as a remarkably high specific surface area (SSA) reaching 3000 m^2/g and a well-defined micropore

Table 2. Textural properties for all produced adsorbent materials and milled raw cork.

Material	S_{BET} (m^2/g)	S_{mic} (m^2/g)	V_t (cm^3/g)	V_{mic} (cm^3/g)	D_p (nm)
Milled cork	5	<LOD	0.03	0.00	1.63
CC1	203	122	0.14	0.06	2.36
CC2	64	<LOD	0.08	0.00	2.41
CCB1	2057	1195	1.21	0.58	2.68
CCB2	1687	1073	1.02	0.53	4.71

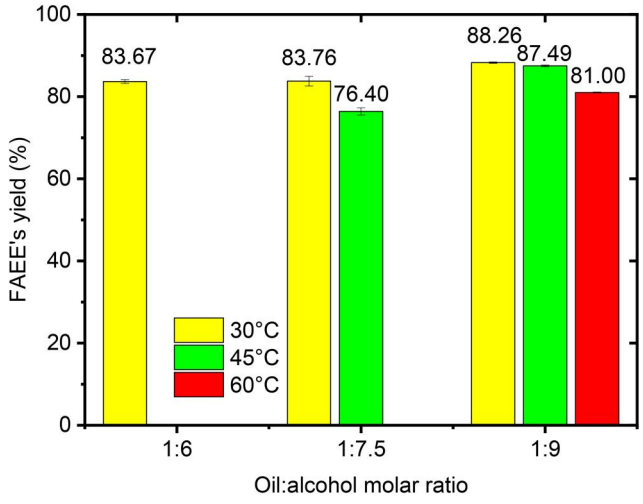

Figure 1. Fatty acid ethyl esters (FAEEs) yield in produced biodiesel as a function of three reaction temperatures (30, 45, and 60 °C) and three oil:alcohol molar proportions (1:6, 1:7.5, and 1:9).

size distribution [23,35,36]. The activation process plays a crucial role in shaping the microporous structure of the resulting biochar, facilitating the development of porosity and the prevalence of acidic and basic functional groups on its surface [36]. Similar values are found in the literature for the surface area of milled raw cork and physically and chemically activated carbons with KOH [19,37,38].

For cork residues without any treatment, surface areas from 1.60 [19] to 3.10 m^2/g [37] are found in the literature. This value varies according to the tree of origin of the cork.

The air-physically activated carbons, CC1 and CC2, presented higher surface areas compared to milled raw cork, implying that the temperature affects the formation of a well-developed porous structure due to more volatile mass escaping from the samples [38]. As the micropore volume increases for CC1, its surface area also increases. In CC2, the micropore volume stays the same as that of milled raw cork, indicating that the carbonization time is a decisive parameter and can prejudice the sample's surface area.

Strong et al. [39] studied the effects of activation time in KOH-activated carbons, showing that the time increase causes pore widening, forming mesopores, and decreasing the surface area. Wang et al. [38] produced physically activated carbon from milled raw cork, with a carbonization of 1.5 h at 500 °C, and achieved a surface area of 270 m^2/g.

The activation process generated CCB1 and CCB2, which presented surface areas 10 and 26 times higher than their precursors, CC1 and CC2, respectively. When chemically activated due to dehydration and degradation of lignocellulosic biomass, activators can increase porosity and enrich chemical groups on their surface, especially when using alkaline solid activators [40]. The overall mechanism involves several reactions that generate high porosity through gas generation at various active sites. It has been shown that chemical activation after pyrolysis or carbonization is crucial to obtaining a large surface area [41]. Wang et al. [19] obtained a material with 2864 m^2/g of BET surface area using pre-carbonized cork at 550 °C for 1 h as a precursor and activating using KOH and carbonization at 750 °C for 2 h.

The plots obtained through thermogravimetric analysis are shown in Figure 2a, 2b, 2c and 2d for CC1, CC2, CCB1, and CCB2 materials, respectively. The black line represents the weight as a function of temperature (solid and dash lines, respectively), and the blue line represents the mass variation (DTG, derivative thermogravimetric curves) as a function of temperature.

TGA under a nitrogen flow demonstrates the thermal stability of the materials. All the prepared samples exhibit notable thermal stability. Significant mass loss occurs around 600 °C for CC1 and CC2, while CCB1 and CCB2 show decomposition after 800 °C. This indicates that materials prepared with KOH at 750 °C (CCB1 and CCB2) possess greater thermal resistance compared to those synthesized at 550 °C (CC1 and CC2), aligning with the higher preparation temperature of the former materials.

Table 3 summarizes the pH_{PZC}, elemental, proximate (and ultimate) analysis of cork, CC1, CC2, CCB1, and CCB2.

In all samples, the main element present is carbon. For the milled raw cork, similar values have been found by Castellar et al. [42], in which the composition is 61.7, 7.7, 0.68, and 29.8 in weight percentage for C, H, N, and O, respectively.

All activated carbons presented, CC1, CC2, CCB1, and CCB2, have a higher carbon content and minor hydrogen and oxygen content compared to milled cork raw due to the decarboxylation and dehydration reaction during carbonization [43]. Physical and chemically activated cork charcoal composition has been analyzed by Wang et al. and presented the same behavior after pyrolysis [37].

The ash content in milled raw cork is usually below 3%, but it can vary depending on the tree [44]. In the present study, the ash content was found to be 0.93% in mass. Additionally, the ash content in the activated carbon samples was higher than in milled raw cork. This behavior is expected since organic matter is lost during carbonization, and inorganic matter becomes more concentrated. The ash content increased from 0.93% in milled raw cork to 2.07% in CC1 and 8.86% in CCB1.

As expected, materials prepared at 550 °C (CC1 and CC2) exhibit higher volatile matter content, while activated carbons prepared at 750 °C (CCB1 and CCB2) show increased fixed carbon levels. The decrease in volatile matter after pyrolysis is attributed to the oxidation reaction between the volatiles released from the activated carbon and KOH [45]. The values are also similar to those reported in the literature [46].

The reduction in volatile matter results in an increased fixed carbon content. Notably, the CCB1 material exhibits the highest fixed carbon content at 71.6 wt.%. This characteristic could be linked to its adsorption capacity, as a higher fixed carbon content tends to enhance adsorption performance [47]. Therefore, CCB1 shows great potential as a material for biodiesel purification.

The molar ratios of H/C and O/C serve as key indicators of the carbonization process. As depicted in the Van Krevelen diagram (see supplementary material), carbonization is marked by a reduction in these ratios, due to the degradation of easily

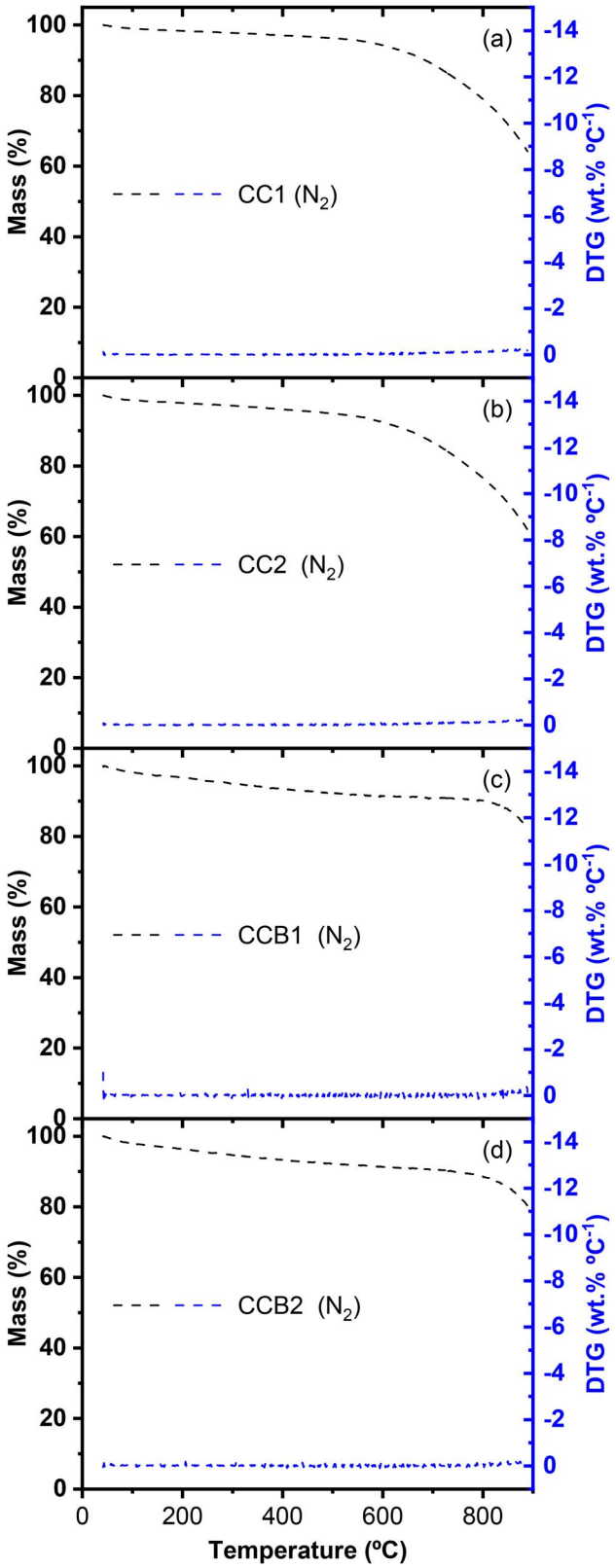

Figure 2. Thermogravimetric analysis of (a) CC1, (b) CC2, (c) CCB1 and (d) CCB2 prepared materials.

decomposable organic matter and the reduction of low-energy bonds, such as H–C and O–C. This trend highlights the prominent roles of dehydration mechanisms during pyrolysis, which significantly reduces the oxygen and hydrogen content, increasing the carbon content [38,48]. The values obtained in this study are consistent with the findings of Wang et al. [38], which demonstrate the effect of carbonization on cork samples, leading to a reduction in the H/C and O/C ratios. In their work, these ratios decreased from 1.46 to 0.39 and from 0.36 to 0.07, respectively, when cork was carbonized at 550 °C. These values can be compared with the milled raw cork H/C and O/C, that started at 1.55 and 0.37, respectively, and decreased to around 0.33 and 0.15 when turned into CC1 and CC2.

Table 3. Elemental, ultimate, and proximate analysis (%wt.) and pH_{PZC} of the samples.

	wt.%								Atomic ratio		
Sample	N	C	H	O[a]	Ashes	Moisture	Volatile matter	Fixed carbon[b]	H/C	O/C	pH_{PZC}
Milled cork	0.46 ± 0.00	60.84 ± 0.13	7.84 ± 0.05	29.93	0.93	–	–	–	1.55	0.37	4.64 ± 0.15
CC1	1.74 ± 0.05	78.08 ± 2.49	2.12 ± 0.06	15.99	2.07	1.20	35.8	60.9	0.33	0.15	10.47 ± 0.05
CC2	1.70 ± 0.09	76.80 ± 4.05	2.01 ± 0.13	13.97	5.52	1.60	38.1	54.8	0.31	0.14	10.40 ± 0.02
CCB1	0.57 ± 0.01	72.71 ± 1.98	0.54 ± 0.04	17.32	8.86	1.50	18.0	71.6	0.09	0.16	9.76 ± 0.00
CCB2	0.60 ± 0.01	72.54 ± 2.53	0.53 ± 0.04	13.86	12.47	2.00	19.7	65.8	0.09	0.14	8.71 ± 0.02

[a]O = 100 – N – C – H – Ashes.
[b]FC = 100 – Moisture – Ashes – Volatile matter.

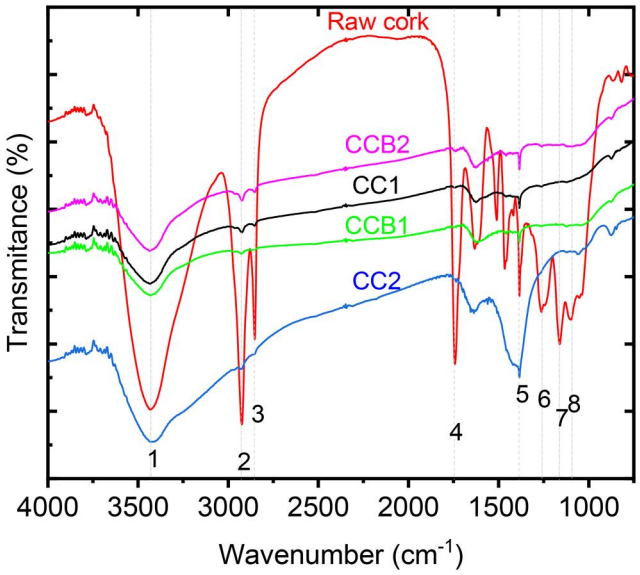

Figure 3. Comparison between milled raw cork and the four prepared adsorbents using FTIR spectroscopy.

The discrepancy in the O/C ratios are related to the high oxygen content of the materials (13.86–17.32 wt.%) compared to the literature and is due to the use of air as physical activating agent presence [49,50].

The pH_{PZC} values are also consistent with the ones found in the literature. Cork samples presented from 3.6 to 4.2 in the works of Fiol and Villaescusa [51] and Wang et al. [37], respectively, changing in accord with the methodology used, but always an acid pH_{PZC}.

Regarding the chemically activated carbon materials, the PZC was basic, and there are three main reasons for this behavior. First, the carbonization process decreases oxygen content, as shown in the elemental composition, and removing the oxygen makes the material surface more basic. Secondly, the ashes, which typically consist on alkaline metals, increased for activated carbon materials respect to the cork raw precursor [52]. Also, the chemical activation is made with a strong base, KOH, which helps increase pH_{PZC}. The decrease of CCB1 and CCB2 PZCs about their precursors CC1 and CC2 may occur because the chemically activated ones are washed until neutral pH, decreasing the PZC value [53]. For values lower than the PZC, removing adsorbates with anionic characteristics can reach more significant values. At pH higher than the PZC, the adsorption of contaminants with a positive charge is favored.

As biodiesel is a non-polar organic phase, adjusting its pH by adding acidic or basic aqueous solutions leads to two immiscible phases. Therefore, pH_{PZC} data were not used in the adsorption of biodiesel, as the formation of two phases would make the adsorption process unfeasible. However, it was studied because it is helpful in the case of using cork and activated carbon in other adsorption processes in an aqueous solution.

Additionally to the pH_{PZC}, the FTIR spectra obtained from milled raw cork and activated carbon samples were analyzed to identify qualitatively the functional groups present in each sample. The data obtained is shown in Figure 3, and the bands are described in the supplementary material, which shows that each band corresponds to a specific functional group.

Upon analysis, in comparison with the precursor material, some of the peaks in the FTIR spectra of the activated carbon samples could not be identified, and some became less intense. This can be

attributed to the degradation of some components, such as suberin, hemicellulose, and cellulose (bands 2, 3, and 4), in the milled raw cork as the temperature exceeds 500 °C during the carbonization process [54].

The changes in the FTIR spectra of the activated carbon samples compared to the milled raw cork can be attributed to the significant changes in the chemical composition and structure of the material during the carbonization process [55]. This is further supported by pH_{PZC} analysis, which shows that certain bands in the raw cork sample, specifically bands 4, 6, and 7, indicate its acidity. The destruction of these functional groups during carbonization results in basic materials and leads to the formation of a relatively stable aromatic carbon structure [47].

Above 350 °C, the FTIR spectra are dominated by the growth of a featureless band in the $1500-1000\,cm^{-1}$ region, indicating the transformation of cork into char, as also stated in the Van Krevelen diagram [56].

Adsorption studies

Preliminary adsorption measurements

The initial screening measurements focused on the removal efficiency of glycerol to select which materials were suitable for further analysis for adsorption parameters, kinetics, and adsorption equilibrium isotherms. The removal performance of each adsorbent obtained in these preliminary experiments is presented in Figure 4.

The removal of glycerol was significant for all tested materials, with a percentage exceeding 68%. Milled raw cork, which was not treated, achieved a removal rate of 77.4 ± 3.2%. Despite its low surface area, it has all its functional groups and an acidic pH_{PZC}. Vasques et al. [14] conducted a study evaluating the impact of pH_{PZC} on glycerol adsorption and found that the removal of glycerol is higher for materials with acidic pH. In their research, a pH of 9.4 removed around 29%, while a pH of 3.4 increased the removal rate to 83%.

The carbonization of cork to generate CC1 and CC2 materials did not favor adsorption. The carbonization reduces the oxygen functional groups [57] and increases the pH_{PZC}, making the interaction between glycerol and the adsorbent weaker and reducing the removal rate.

However, the activation of CC1 and CC2 with KOH causes the functional groups and surface area to increase substantially [57]. For this reason, although pH_{PZC} remains basic, the increase in area and functional groups compensates for this, making these materials the most effective.

Based on the results presented in Figure 4, CCB1 was the most efficient adsorbent for removal, removing 80.9 ± 3.7% of the glycerol. Therefore, it was selected for further adsorption measurements. Milled raw cork was also used as it had great potential for glycerol removal and was a residue that did not require prior treatment, which is relevant in terms of economic advantages for industrial applications.

Adsorption kinetics

Adsorption kinetics studies were conducted for milled raw cork and CCB1 material at 25, 35, and 45 °C using 2 and 3 wt.% of adsorbent loads. The results are presented in Figure 5, which allows to evaluate the time required for glycerol removal at different temperatures. All experiments achieved the adsorption equilibrium after 360 min (6h).

Lower temperatures favor adsorption using 2% adsorbent in milled cork and CCB1 materials. Anhesine et al. [58] obtained the same results using sugarcane bagasse ash to purify biodiesel. In that work, temperatures from 25 to 65 °C and concentrations from 2 to 6% of adsorbent were studied, and

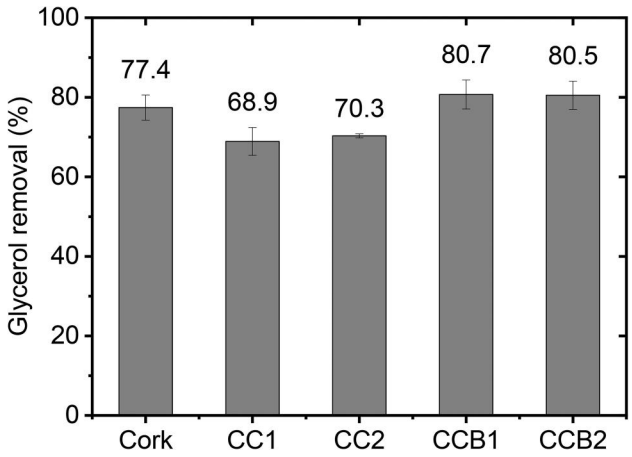

Figure 4. Glycerol removal percentage calculated using milled raw cork, and the four CC1, CC2, CCB1, and CCB2 prepared materials were applied as adsorbents (2.5 wt.%).

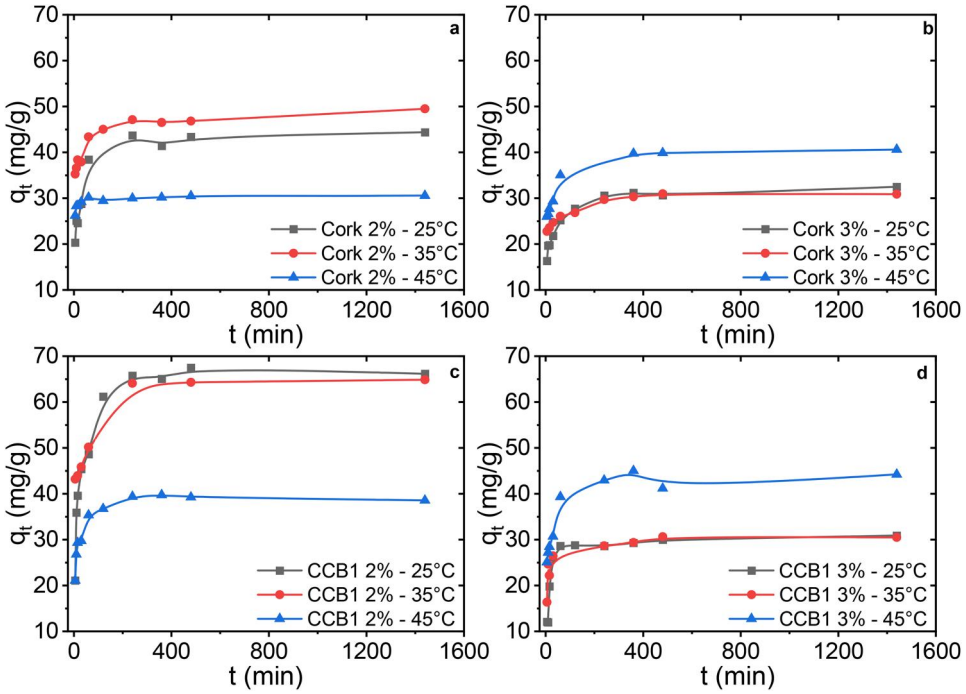

Figure 5. Adsorption kinetics of glycerol at temperatures of 25, 30, and 45 °C using milled raw cork 2 and 3 wt.% (a and b, respectively) and CCB1 2 and 3 wt.% (c and d, respectively) as adsorbent (standard deviation <5%).

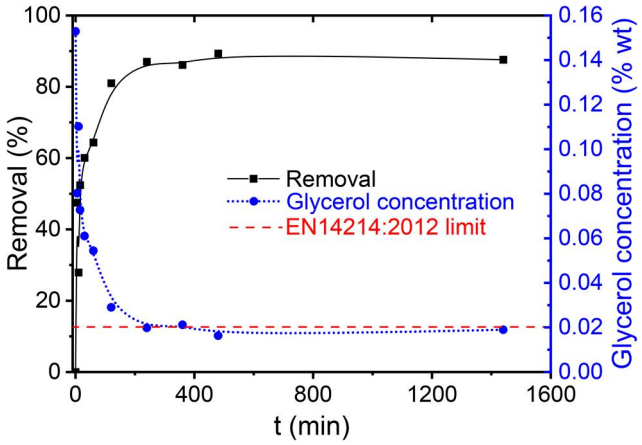

Figure 6. Glycerol removal (solid line) and concentration profile (dotted line) in biodiesel using 2% CCB1 as adsorbent at 25 °C; The horizontal line (dashed) represents the maximum glycerol concentration specified by the Europen Standard EN 14214:2012+A2:2019 (standard deviation <5%).

the best glycerol removal occurred at the lowest temperature and concentration.

Increasing adsorbent concentration impaired adsorption for both materials. The materials' low density makes the volume very large, forming agglomerates of adsorbent and decreasing their surface contact area with the adsorbate. Therefore, its adsorption capacity decreases.

CCB1 showed the most significant removal capacity at 25 °C, reaching a removal value of almost 70 $mg_{glycerol}/g_{biodiesel}$, and milled cork had the most considerable removal at 25 °C of approximately 50 mg/g, both with 2 wt.% of adsorbent. Results presented in Figure 6 show the removal capacity of CCB1 at 25 °C, reaching 0.016 wt.% of glycerol, corresponding to 89% of removal. This value is within the maximum limit of 0.02 wt.% established by the European Standard EN 14214:2012+A2:2019 [6].

PFO, PSO, Elovich, and Weber and Morris kinetic models were adjusted to experimental data. Table 4 shows the parameters for the best fittings. All graphs and estimated parameters using the four kinetic models are presented in the supplementary material.

The first clear conclusion from the analysis of the results presented in Table 4 is that the models that best fit the experimental data are the PSO and the Elovich models. This means that adsorption is governed neither by physisorption nor by intraparticle diffusion mechanisms.

For milled raw cork as adsorbent, it is possible to see that, except for 2% with 35 °C, Elovich is the

Table 4. Estimated parameters and error analysis using four kinetic models for glycerol adsorption kinetics onto milled raw cork and CCB1 for three temperatures (25, 35, and 45 °C) and two adsorbent dosages (2 and 3%).

Material	Dosage (wt.%)	Temperature (°C)	Model	Parameters	Values	$\Delta q_e(\%)$	*Red* χ^2
Milled raw cork	2	25	Elovich	α (mg. g^{-1}.min^{-1})	6.57×10^1	7.936	0.2405
				β (g. mg^{-1})	0.2025		
		35	Elovich	α (mg. g^{-1}.min^{-1})	2.08×10^5	3.122	0.0411
				β (g. mg^{-1})	0.3666		
		45	PSO	k_2 (g.mg^{-1}.min^{-1})	0.0430	1.260	0.0047
				q_e (mg.g^{-1})	30.22		
	3	25	Elovich	α (mg. g^{-1}.min^{-1})	1.24×10^2	4.401	0.0544
				β (g. mg^{-1})	0.3152		
		35	Elovich	α (mg. g^{-1}.min^{-1})	1.41×10^5	2.974	0.0249
				β (g. mg^{-1})	0.5835		
		45	Elovich	α (mg. g^{-1}.min^{-1})	2.22×10^3	4.585	0.0718
				β (g. mg^{-1})	0.3261		
CCB1	2	25	PSO	k_2 (g.mg^{-1}.min^{-1})	0.0015	7.413	0.2622
				q_e (mg.g^{-1})	65.24		
		35	Elovich	α (mg. g^{-1}.min^{-1})	5.24×10^3	6.499	0.2292
				β (g. mg^{-1})	0.2136		
		45	PSO	k_2 (g.mg^{-1}.min^{-1})	0.0059	5.244	0.0865
				q_e (mg.g^{-1})	38.38		
	3	25	PSO	k_2 (g.mg^{-1}.min^{-1})	0.0030	12.67	0.2445
				q_e (mg.g^{-1})	31.07		
		35	PSO	k_2 (g.mg^{-1}.min^{-1})	0.0085	6.295	0.0962
				q_e (mg.g^{-1})	30.02		
		45	Elovich	α (mg. g^{-1}.min^{-1})	4.14×10^2	6.787	0.1866
				β (g. mg^{-1})	0.2508		

Table 5. Comparison of estimated kinetics parameters with previous research (temperature, pseudo-second-order constant, k_2 and equilibrium capacity, q_e).

Adsorbent	Temperature (°C)	k_2 (g.$mg^{-1}min^{-1}$)	q_e (mg.g^{-1})	Reference
Passion fruit seeds	60	0.106	4.263	[16]
Sugarcane bagasse	30	0.0763	8.163	[11]
Commercial AC	30	0.000082	29.4	[14]
CCB1	25	0.0015	65.2	This study

model that best fits the experimental data. The best fittings for cork adsorption proceeded from the experiment with 2 wt.% at 45 °C, where the model reached a standard normalized error of 1.26%, an estimated value for q_e of 30.22 mg.g^{-1} and a velocity constant, k_2 of 0.0430 g.$mg^{-1}min^{-1}$ for PSO model.

For CCB1 material as adsorbent, except for the cases of 2% with 35 °C and 3% with 45 °C, PSO is the model that best fits the experimental data. The PSO model depends on the amount of adsorbate on the surface of the adsorbent and the amount of adsorbate at equilibrium. The adsorption rate is proportional to the square of the number of active sites on the surface. In this adsorption type, exchanges occur specifically in the active centers, initially forming a single layer. However, other layers may be formed by physisorption [59]. The PSO model describes the adsorption process through chemical and rate control, suggesting that adsorption efficiency depends on the availability of active sites in the adsorbent. Unlike the PFO, this model considers the interaction mechanism between adsorbate and adsorbent as the rate-determining step, relying on physical-chemical interactions between entities to describe a chemisorption process. For CCB1, the best fitting was in the experiment using 2 wt.% at 45 °C, where CCB1 reached a standard normalized error of 5.24% an estimated q_e value of 38.38 mg.g^{-1} and a velocity constant of 0.0059 g.$mg^{-1}min^{-1}$ using the PSO model. Paschoal et al. [16] studied glycerol adsorption in biodiesel and showed that, in the same conditions, the two models present approximately the same results for q_e while the velocity constant drops from PFO to PSO. The experiment using 2 wt.% at 25 °C of CCB1 was the one that achieved the highest level of purification, using the conditions that most favored the adsorption into the activated carbon. In this, CCB1 material allows estimating a q_e value of 65.24 mg.g^{-1} using the pseudo-second-order model.

Results presented in Table 5 show the glycerol in biodiesel adsorption capacity and velocity constants for some adsorbents compared to those in this study.

Compared to CCB1, the adsorption capacity of cork-activated carbon is more significant, being 2.3, 8.2, and 15.7 times higher than the adsorption capacity of a commercial adsorbent, sugarcane bagasse, and passion fruit seed bran, the adsorbents used by Vasques et al. [14], Alves et al. [11] and Paschoal et al. [16].

Equilibrium adsorption isotherms

The equilibrium adsorption isotherm measurements were made at 25, 35, and 45 °C temperatures with

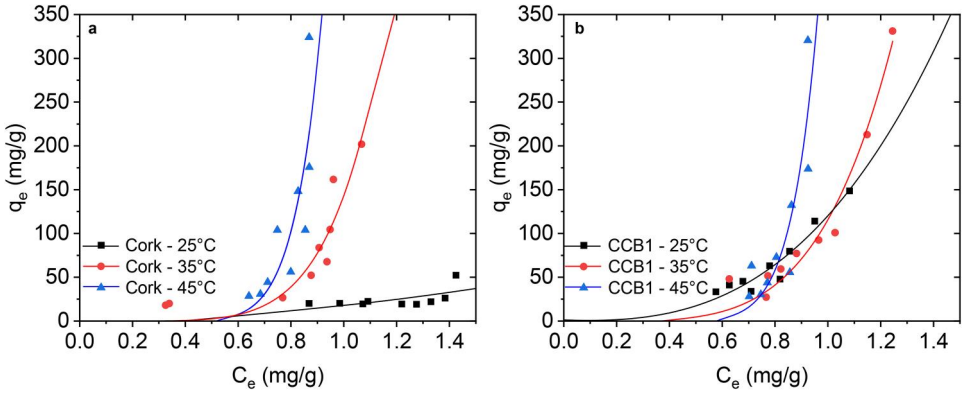

Figure 7. Adsorption equilibrium isotherms for glycerol removal using milled raw cork (a) and CCB1 (b) as adsorbent for 25, 35, and 45 °C temperatures (standard deviation <5%).

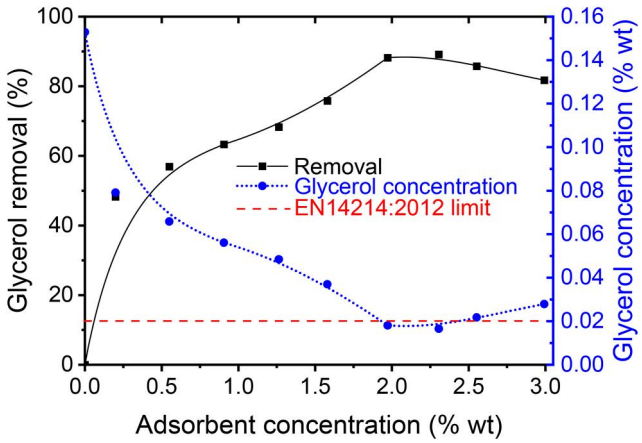

Figure 8. Effect of CCB1 adsorbent concentration on glycerol removal and purified biodiesel glycerol content; the red line shows the limit specified by EN 14214:2012+A2:2019 standard (standard deviation <5%).

milled raw cork and the selected CCB1 material as adsorbents to evaluate the best adsorbent capacity in glycerol removal. Figure 7 shows the influence of temperature and adsorbent load on adsorption capacity, q_e, for milled raw cork (a) and CCB1 material (b), respectively.

From the analysis of the results presented in the figure, it can be noted that the adsorption isotherms are S1-type, representing unfavorable isotherms [60]. This type of isotherm shows that adsorption is more considerable at high concentrations and was also found in studies on biodiesel purification by adsorption by Vasques et al. and Pachoal et al. [14,16].

The S1-curves are typically observed when the adsorbate is monofunctional (adsorbs as a unit) and has moderate intermolecular interactions associated with competition for adsorption sites [61]. Interactions between adsorbate molecules can cause this, as glycerol has difficulty accessing the adsorbent surface due to competition for adsorption sites by other molecules (soap, free fatty acid residues, and ethanol) and facilitated by the diffusion resistance of biodiesel, mainly at low temperatures, as can be observed for milled raw cork isotherms. This model also predicts the formation of multiple layers, which is expected, given the cooperative adsorption between glycerol molecules. Paschoal et al. [16] studied glycerol adsorption in biodiesel using passion fruit seeds as an adsorbent and also found a S1-type behavior in equilibrium isotherms.

Like the kinetic experiments, the best removal in the isotherms occurred with activated carbon CCB1 at 25 °C. The plot presented in Figure 8 shows glycerol removal and its mass percentage at different adsorbent concentrations.

For concentrations above 2 wt.%, the adsorption process is impaired by the large volume of adsorbent in the test. In this way, the removal drops, and the percentage of glycerol remains high. The best results were obtained with 2 and 2.3 wt.% of adsorbent, where the removal was 88 and 89%, and glycerol content was 0.018 and 0.017% by mass, respectively.

The equilibrium isotherm models of Freundlich, Langmuir, Toth, Radke-Prusnitz, and Sips were adjusted to experimental data; the graphs can be found in the supplementary material. Other models were also considered, but these results were not shown due to the negative estimated parameters. The results obtained by fitting the five previously referred models show that Langmuir and Toth models do not describe the equilibrium adsorption

isotherm behavior for none of the studied operational conditions. The Langmuir model, built upon the premise of monolayer adsorption on a uniform surface, fails to describe unfavorable adsorption. This limitation stems from its inability to accommodate systems featuring multilayer adsorption or heterogeneous surfaces, like the assumption of Toth model, where unfavorable adsorption behavior is prevalent.

Freundlich, Radke-Prusnitz, and Sips models satisfactorily describe the experimental isotherms adsorption process of glycerol on milled raw cork and CCB1 adsorbent, except for milled raw cork at 25 °C. The best fitting was obtained for CCB1 adsorbent at 25 °C with a normalized standard error of 23.4% and a reduced Qui-squared of 2.98, as presented in Table 6.

The three adjusted isotherms, while different in formulation, can result in similar curves under low concentrations. When $C_e \rightarrow 0$, the Sips isotherm simplifies to $q_e = Q_s K_s C_e^{n_s}$, which mirrors the Freundlich form when $n_s = n_F^{-1}$. Likewise, the Radke-Prausnitz isotherm, under low concentrations, reduces to $q_e = BC_e^{\beta}$, becoming equivalent to Freundlich when $\beta = n_F^{-1}$. In summary, all three describe adsorption at low concentrations with a power-law dependency on the solute concentration, resembling the Freundlich model [29,62]. The bold values shown in Table 6 confirm the equivalence of the curves.

Since estimated parameters using Freundlich, Radke-Praunistz, and Sips models are equivalent in terms of normalized standard deviation error it is possible to discuss results based on Freundlich parameters. Thus, K_F represents a measure of the adsorption strength, while n is related to the energy heterogeneity of the adsorbent surface. They depend on temperature, pH value, amount of adsorbent, and concentration range. When $0 < n_F < 1$, a concave

Table 6. Freundlich, Radke-Prausnitz and Sips estimated parameters for glycerol equilibrium adsorption isotherms onto cork and CCB1 adsorbents for 25, 35, and 45 °C.

Adsorbent	Model	Temperature (°C)	Parameters	Values	$\Delta q_e(\%)$	*Red* χ^2
Milled raw cork	Freundlich	25	K_F ($g.g^{-1}$)	19.91	23.05	2.391
			n_F^{-1}	**1.824**		
		35	K_F ($g.g^{-1}$)	129.5	56.46	9.865
			n_F^{-1}	**6.020**		
		45	K_F ($g.g^{-1}$)	298.6	37.84	24.82
			n_F^{-1}	**6.692**		
	Radke-Prausnitz	25	A ($g.g^{-1}$)	1.097×10^7	23.05	2.391
			B (($mg.g^{-1}$).($mg.mg^{-1}$)$^{-\beta}$)	17.76		
			β	**1.818**		
		35	A ($g.g^{-1}$)	9.227×10^6	56.46	9.865
			B (($mg.g^{-1}$).($mg.mg^{-1}$)$^{-\beta}$)	129.5		
			β	**6.021**		
		45	A ($g.g^{-1}$)	4.879×10^7	37.84	24.82
			B (($mg.g^{-1}$).($mg.mg^{-1}$)$^{-\beta}$)	298.5		
			β	**5.693**		
	Sips	25	Q_S ($mg.g^{-1}$)	1.458×10^3	23.05	2.392
			K_S ($g.mg^{-1}$)	0.0123		
			n_S	**1.845**		
		35	Q_S ($mg.g^{-1}$)	4.050×10^4	56.46	9.877
			K_S ($g.mg^{-1}$)	0.0032		
			n_S	**6.036**		
		45	Q_S ($mg.g^{-1}$)	1.916×10^4	37.85	24.87
			K_S ($g.mg^{-1}$)	0.0157		
			n_S	**5.714**		
CCB1	Freundlich	25	K_F ($g.g^{-1}$)	105.4	23.39	2.978
			n_F^{-1}	**2.472**		
		35	K_F ($g.g^{-1}$)	110.9	33.26	7.073
			n_F^{-1}	**4.003**		
		45	K_F ($g.g^{-1}$)	221.0	41.09	23.98
			n_F^{-1}	**6.116**		
	Radke-Prausnitz	25	A ($g.g^{-1}$)	1.097×10^7	23.39	2.979
			B (($mg.g^{-1}$).($mg.mg^{-1}$)$^{-\beta}$)	105.4		
			β	**2.472**		
		35	A ($g.g^{-1}$)	1.097×10^7	33.26	7.073
			B (($mg.g^{-1}$).($mg.mg^{-1}$)$^{-\beta}$)	110.9		
			β	**6.021**		
		45	A ($g.g^{-1}$)	1.097×10^7	44.38	27.98
			B (($mg.g^{-1}$).($mg.mg^{-1}$)$^{-\beta}$)	221.0		
			β	**6.117**		
	Sips	25	Q_S ($mg.g^{-1}$)	1.547×10^4	23.41	3.008
			K_S ($g.mg^{-1}$)	0.0068		
			n_S	**2.478**		
		35	Q_S ($mg.g^{-1}$)	6.608×10^4	33.28	7.110
			K_S ($g.mg^{-1}$)	0.0017		
			n_S	**4.005**		
		45	Q_S ($mg.g^{-1}$)	2.388×10^4	44.40	27.98
			K_S ($g.mg^{-1}$)	0.0093		
			n_S	**6.140**		

curve is formed ($n_F^{-1} > 1$). It represents unfavorable adsorption and can lead to a relatively long mass transfer path in fixed beds [61]. A lower value of $n_F < 1$ indicates that the adsorbent works well for high-concentration solutions; however, the high value of n ($n_F > 1$) shows the potential adsorption capacity of adsorbent for low-concentration solutions [63]. The n_F values found were consistent with the behavior presented since they are less than 1, representing an unfavorable adsorption. For glycerol adsorption onto milled raw cork and CCB1 material, the effect of temperature is notable. As temperature increases, K_F value increases and n_F value decreases. This tendency was also noted by Paschoal et al. [16]. The Freundlich model assumes that the surface is heterogeneous and irregular, and the adsorption distribution is described with non-uniform energies. It also predicts cooperative adsorption between glycerol molecules and anticipates the formation of a multilayer over milled raw cork and CCB1 material adsorbents.

Conclusions

The study explored sustainable biodiesel purification using cork waste-derived adsorbents as an alternative to water washing, and the main findings were:

- Optimal biodiesel production was achieved at 30 °C, 1:9 oil:alcohol molar ratio, 1 wt.% NaOH catalyst, with a 1-hour reaction time, yielding 88.26 wt.% of FAEEs with a glycerol content of 0.1529 wt.%;
- Four cork-based adsorbents (2 physical, 2 chemical) were developed, reaching up to 2057 m^2/g BET surface area after chemical activation;
- The models that more fits to adsorption kinetics were Elovich and pseudo-second order for adsorption using milled raw cork and the activated carbon CCB1, respectively;
- The equilibrium isotherms presented an unfavorable behavior, and therefore the model that fitted best to the data was from Freundlich;
- The material CCB1 (carbonized with air and KOH) showed the highest glycerol removal efficiency (88%) at 25 °C, 2 wt.% dosage, and 6-hour contact time, with a glycerol content of 0.016 wt.% after adsorption;
- This method meets the requirements of the EN 14214:2012+A2:2019 standards, offering a low-cost, eco-friendly alternative to conventional biodiesel purification.

Acknowledgments

The authors acknowledge the Department of Chemical and Environmental Technology (ESCET) at Rey Juan Carlos University and LAMAP (Multiuser Research Support Laboratory from UTFPR-Apucarana, Brazil) for the material analysis, and Amorim Cork Composites for the kindly supply of cork powder residues.

Disclosure statement

No potential conflict of interest was reported by the author(s).

Funding

This work was supported by national funds through FCT/MCTES (PIDDAC): CIMO, UIDB/00690/2020 (DOI: 10.54499/UIDB/00690/2020) and UIDP/00690/2020 (DOI: 10.54499/UIDP/00690/2020); and SusTEC, LA/P/0007/2020 (DOI: 10.54499/LA/P/0007/2020). Jose L. Diaz De Tuesta acknowledges the financial support through the program of Atracción al Talento of Comunidad de Madrid (Spain) for the individual research grant and project 2022-T1/AMB-23946.

ORCID

Maria Isabella Lima Garção http://orcid.org/0000-0002-0850-1139
Gabriel Lamino Camilo http://orcid.org/0000-0002-3797-0356
Jose L. Diaz De Tuesta http://orcid.org/0000-0003-2408-087X
Maria Carolina Sérgi Gomes http://orcid.org/0000-0003-2210-0275
Paulo Brito http://orcid.org/0000-0003-1805-0252

References

[1] Gebremariam SN, Marchetti JM. Economics of biodiesel production. Energy Convers Manage. 2018; 168:74–84. doi: 10.1016/j.enconman.2018.05.002.
[2] Cabrera-Jiménez R, Mateo-Sanz JM, Gavaldà J, et al. Comparing biofuels through the lens of sustainability: a data envelopment analysis approach. Appl Energy. 2022;307:118201. doi: 10.1016/j.apenergy.2021.118201.
[3] Foroutan R, Esmaeili H, Mousavi SM, et al. The physical properties of biodiesel-diesel fuel produced via transesterification process from different oil sources. Phys Chem Res. 2019;7:415–424.
[4] Liu L, Mu B, Li W, et al. Clean cotton dyeing in circulated dyebath of waste cooking oil: a feasible industrialization strategy for pollution minimization. J Cleaner Prod. 2021;278:123799. doi: 10.1016/j.jclepro.2020.123799.
[5] Moazeni F, Chen Y-C, Zhang G. Enzymatic transesterification for biodiesel production from used cooking oil, a review. J Cleaner Prod. 2019;216:117–128. doi: 10.1016/j.jclepro.2019.01.181.
[6] European Committee for Standardization, European Standard EN14214:2012+A2:2019. Liquid petroleum products - Fatty acid methyl esters (FAME) for use in diesel engines and heating applications -

Requirements and test methods. 2019. https://standards.cencenelec.eu/dyn/www/f?p=CEN:110:0::::FSP_PROJECT,FSP_ORG_ID:68664,6003&cs=19A9C4EEEAC250EA2A8EC28687DC479AB

[7] Carmona-Cabello M, García IL, Papadaki A, et al. Biodiesel production using microbial lipids derived from food waste discarded by catering services. Bioresour Technol. 2021;323:124597. doi: 10.1016/j.biortech.2020.124597.

[8] Saleh J, Tremblay AY, Dubé MA. Glycerol removal from biodiesel using membrane separation technology. Fuel. 2010;89(9):2260–2266. doi: 10.1016/j.fuel.2010.04.025.

[9] Chozhavendhan S, Singh MVP, Fransila B, et al. A review on influencing parameters of biodiesel production and purification processes. Curr Res Green Sustainable Chem. 2020;1–2:1–6. doi: 10.1016/j.crgsc.2020.04.002.

[10] Atadashi I. Purification of crude biodiesel using dry washing and membrane technologies. Alexandria Eng J. 2015;54(4):1265–1272. doi: 10.1016/j.aej.2015.08.005.

[11] Alves MJ, Cavalcanti ÍV, de Resende MM, et al. Biodiesel dry purification with sugarcane bagasse. Ind Crops Prod. 2016;89:119–127. doi: 10.1016/j.indcrop.2016.05.005.

[12] Manique MC, Faccini CS, Onorevoli B, et al. Rice husk ash as an adsorbent for purifying biodiesel from waste frying oil. Fuel. 2012;92(1):56–61. doi: 10.1016/j.fuel.2011.07.024.

[13] Farid MAA, Hassan MA, Taufiq-Yap YH, et al. Waterless purification using oil palm biomass-derived bioadsorbent improved the quality of biodiesel from waste cooking oil. J Cleaner Prod. 2017;165:262–272. doi: 10.1016/j.jclepro.2017.07.136.

[14] de Castro Vasques É, Granhen Tavares CR, Itsuo Yamamoto C, et al. Adsorption of glycerol, monoglycerides and diglycerides present in biodiesel produced from soybean oil. Environ Technol. 2013;34:2361–2369. doi: 10.1080/21622515.2013.770558.

[15] Bateni H, Saraeian A, Able C. A comprehensive review on biodiesel purification and upgrading. Biofuel Res J. 2017;4(3):668–690. doi: 10.18331/BRJ2017.4.3.5.

[16] Paschoal SM, Sgorlon JG, Gama L, et al. Application of passion fruit seed meal in alternative biodiesel purification process: study of glycerol adsorption mechanism and incorporation into polymeric membrane. Biofuels. 2023;14(9):957–966. doi: 10.1080/17597269.2023.2194117.

[17] Sandouqa A, Al-Shannag M, Al-Hamamre Z. Biodiesel purification using biomass-based adsorbent manufactured from delignified olive cake residues. Renewable Energy. 2020;151:103–117. doi: 10.1016/j.renene.2019.11.009.

[18] Wang Q, Lai Z, Mu J, et al. Converting industrial waste cork to biochar as Cu (II) adsorbent via slow pyrolysis. Waste Manag. 2020;105:102–109. doi: 10.1016/j.wasman.2020.01.041.

[19] Wang Q, Lai Z, Luo C, et al. Honeycomb-like activated carbon with microporous nanosheets structure prepared from waste biomass cork for highly efficient dye wastewater treatment. J Hazard Mater. 2021;416:125896. doi: 10.1016/j.jhazmat.2021.125896.

[20] Sørensen IH, Torralba M, Quintas-Soriano C, et al. Linking cork to cork oak landscapes: mapping the value chain of cork production in Portugal. Front Sustainable Food Syst. 2021;5:787045. doi: 10.3389/fsufs.2021.787045.

[21] Mestre AS, Pires RA, Aroso I, et al. Activated carbons prepared from industrial pre-treated cork: sustainable adsorbents for pharmaceutical compounds removal. Chem Eng J. 2014;253:408–417. doi: 10.1016/j.cej.2014.05.051.

[22] Novais RM, Caetano APF, Seabra MP, et al. Extremely fast and efficient methylene blue adsorption using eco-friendly cork and paper waste-based activated carbon adsorbents. J Cleaner Prod. 2018;197:1137–1147. doi: 10.1016/j.jclepro.2018.06.278.

[23] Kopac T. Hydrogen storage characteristics of biobased porous carbons of different origin: a comparative review. Int J Energy Res. 2021;45(15):20497–20523. doi: 10.1002/er.7130.

[24] Camilo GL, Queiroz A, Ribeiro AE, et al. Review of biodiesel production using various feedstocks and its purification through several methodologies, with a specific emphasis on dry washing. J Ind Eng Chem. 2024;136:1–15. doi: 10.1016/j.jiec.2024.02.016.

[25] Oraegbunam JC, Ishola NB, Sotunde BA, et al. Sandbox oil biodiesel production modeling and optimization with neural networks and genetic algorithm. Green Technol Sustainability. 2023;1(1):100007. doi: 10.1016/j.grets.2022.100007.

[26] European Committee for Standardization, European Standard. EN14103:2020. Fat and oil derivatives. Fatty acid methyl esters (FAME). Determination of ester and linolenic acid methyl ester contents. 2020. https://standards.cencenelec.eu/dyn/www/f?p=CEN:110:0::::FSP_PROJECT,FSP_ORG_ID:64092,6288&cs=19F16C6155234E84BF547D270F4B44D71

[27] Rovani S, Rodrigues AG, Medeiros LF, et al. Synthesis and characterisation of activated carbon from agroindustrial waste—preliminary study of 17β-estradiol removal from aqueous solution. J Environ Chem Eng. 2016;4(2):2128–2137. doi: 10.1016/j.jece.2016.03.030.

[28] Bondioli P, Della Bella L. An alternative spectrophotometric method for the determination of free glycerol in biodiesel. Eur J Lipid Sci Technol. 2005;107(3):153–157. doi: 10.1002/ejlt.200401054.

[29] Sips R. On the structure of a catalyst surface. J Chem Phys. 1948;16(5):490–495. doi: 10.1063/1.1746922.

[30] Wang J, Guo X. Adsorption kinetic models: physical meanings, applications, and solving methods. J Hazard Mater. 2020;390:122156. doi: 10.1016/j.jhazmat.2020.122156.

[31] Baysal M, Bilge K, Yılmaz B, et al. Preparation of high surface area activated carbon from waste-biomass of sunflower piths: kinetics and equilibrium studies on the dye removal. J Environ Chem Eng. 2018;6(2):1702–1713. doi: 10.1016/j.jece.2018.02.020.

[32] Benjumea P, Agudelo JR, Agudelo AF. Effect of the degree of unsaturation of biodiesel fuels on engine performance, combustion characteristics, and emissions. Energy Fuels. 2011;25(1):77–85. doi: 10.1021/ef101096x.

[33] Gomes MCS, Arroyo PA, Pereira NC. Biodiesel production from degummed soybean oil and glycerol removal using ceramic membrane. J Membr Sci.

2011;378(1–2):453–461. doi: 10.1016/j.memsci.2011.05.033.
[34] Da Silva Neto DL, Loz Ferreira PV, Soletti JI, et al. Factorial design and surface method to optimization ethylic biodiesel production from chicken wastes. Chem Ind Chem Eng Q. 2021;27(2):155–163. doi: 10.2298/CICEQ191117034S.
[35] Kopac T. Current overview of the valorization of bio-wastes for adsorbed natural gas applications. Carbon Lett. 2023;33(6):1519–1547. doi: 10.1007/s42823-023-00508-0.
[36] Jedynak K, Charmas B. Adsorption properties of biochars obtained by KOH activation. Adsorption. 2024;30(2):167–183. doi: 10.1007/s10450-023-00399-7.
[37] Wang Q, He D, Li C, et al. Honeycomb-like cork activated carbon modified with carbon dots for high-efficient adsorption of Pb(II) and rhodamine B. Ind Crops Prod. 2023;196:116485. doi: 10.1016/j.indcrop.2023.116485.
[38] Wang Q, Chu D, Luo C, et al. Transformation mechanism from cork into honeycomb–like biochar with rich hierarchical pore structure during slow pyrolysis. Ind Crops Prod. 2022;181:114827. doi: 10.1016/j.indcrop.2022.114827.
[39] Strong OK, Nazari E, Roy T, et al. Transforming micropores to mesopores by heat cycling KOH activated petcoke for improved kinetics of adsorption of naphthenic acids. Heliyon. 2023;9(2):e13500. doi: 10.1016/j.heliyon.2023.e13500.
[40] Panwar NL, Pawar A. Influence of activation conditions on the physicochemical properties of activated biochar: a review. Biomass Convers Biorefin. 2022;12(3):925–947. doi: 10.1007/s13399-020-00870-3.
[41] Ouyang J, Zhou L, Liu Z, et al. Biomass-derived activated carbons for the removal of pharmaceutical mircopollutants from wastewater: a review. Sep Purif Technol. 2020;253:117536.
[42] Castellar J, Formosa J, Fernández AI, et al. Cork as a sustainable carbon source for nature-based solutions treating hydroponic wastewaters – Preliminary batch studies. Sci Total Environ. 2019;650(Pt 1):267–276. doi: 10.1016/j.scitotenv.2018.08.365.
[43] Gascó G, Paz-Ferreiro J, Álvarez ML, et al. Biochars and hydrochars prepared by pyrolysis and hydrothermal carbonisation of pig manure. Waste Manag. 2018;79:395–403. doi: 10.1016/j.wasman.2018.08.015.
[44] Engel JB, Luchese CL, Tessaro IC. Characterization techniques comparison towards a better understanding of different cork-based stoppers types. J Food Eng. 2022;328:111063. doi: 10.1016/j.jfoodeng.2022.111063.
[45] Zhang C, Sun S, Xu S, et al. CO2 capture over steam and KOH activated biochar: effect of relative humidity. Biomass Bioenergy. 2022;166:106608. doi: 10.1016/j.biombioe.2022.106608.
[46] de Mora A, Diaz de Tuesta JL, Pariente MI, et al. Chemically activated hydrochars as catalysts for the treatment of HTC liquor by catalytic wet air oxidation. Catal Today. 2024;429:114462. doi: 10.1016/j.cattod.2023.114462.
[47] Sumaila A, Sumaila AO, Usman AO, et al. Thermal degradation and particle size distribution studies of activated carbon obtained from coconut shells. J Mater Environ Sci. 2022;12:739–746.
[48] de Freitas Batista G, Roman FF, de Tuesta JLD, et al. Assessment of pretreatments for highly concentrated leachate waters to enhance the performance of catalytic wet peroxide oxidation with sustainable low-cost catalysts. Catalysts. 2022;12(2):238. doi: 10.3390/catal12020238.
[49] Sun Z, Dai L, Lai P, et al. Air oxidation in surface engineering of biochar-based materials: a critical review. Carbon Res. 2022;1(1):32. doi: 10.1007/s44246-022-00031-3.
[50] Diaz de Tuesta JL, Saviotti MC, Roman FF, et al. Assisted hydrothermal carbonization of agroindustrial byproducts as effective step in the production of activated carbon catalysts for wet peroxide oxidation of micro-pollutants. J Environ Chem Eng. 2021;9(1):105004. doi: 10.1016/j.jece.2020.105004.
[51] Fiol N, Villaescusa I. Determination of sorbent point zero charge: usefulness in sorption studies. Environ Chem Lett. 2009;7(1):79–84. doi: 10.1007/s10311-008-0139-0.
[52] Sajjadi B, Chen W-Y, Egiebor NO. A comprehensive review on physical activation of biochar for energy and environmental applications. Rev Chem Eng. 2019;35(6):735–776. doi: 10.1515/revce-2017-0113.
[53] Li L, Quinlivan PA, Knappe DR. Effects of activated carbon surface chemistry and pore structure on the adsorption of organic contaminants from aqueous solution. Carbon. 2002;40(12):2085–2100. doi: 10.1016/S0008-6223(02)00069-6.
[54] Pintor AMA, Silvestre-Albero AM, Ferreira CIA, et al. Textural and surface characterization of cork-based sorbents for the removal of oil from water. Ind Eng Chem Res. 2013;52(46):16427–16435. doi: 10.1021/ie402038n.
[55] Ma Z, Yang Y, Wu Y, et al. In-depth comparison of the physicochemical characteristics of bio-char derived from biomass pseudo components: hemicellulose, cellulose, and lignin. J Anal Appl Pyrolysis. 2019;140:195–204. doi: 10.1016/j.jaap.2019.03.015.
[56] Pascoal Neto C, Rocha J, Gil A, et al. 13C solid-state nuclear magnetic resonance and Fourier transform infrared studies of the thermal decomposition of cork. Solid State Nucl Magn Reson. 1995;4(3):143–151. doi: 10.1016/0926-2040(94)00039-F.
[57] Amran F, Zaini MAA. Valorization of Casuarina empty fruit-based activated carbons for dyes removal – Activators, isotherm, kinetics and thermodynamics. Surf Interfaces. 2021;25:101277. doi: 10.1016/j.surfin.2021.101277.
[58] Anhesine MW, dos Santos AV, Pozzi AR, et al. Utilização da cinza do bagaço de cana de açúcar no processo de purificação do biodiesel produzido a partir de óleos e gorduras residuais/Use of sugar cane bagasse ash in the purification of biodiesel production from residual oils and fats. Braz J Dev. 2022;8(2):13720–13745. doi: 10.34117/bjdv8n2-347.
[59] Giles CH, Smith D, Huitson A. A general treatment and classification of the solute adsorption isotherm. I. Theoretical. J Colloid Interface Sci. 1974;47(3):755–765. doi: 10.1016/0021-9797(74)90252-5.
[60] Giles CH, MacEwan TH, Nakhwa SN, et al. Studies in adsorption. Part XI. A system of classification of

solution adsorption isotherms, and its use in diagnosis of adsorption mechanisms and in measurement of specific surface areas of solids. J Chem Soc. 111 (1960) 3973–3993. doi: 10.1039/jr9600003973 .

[61] Hu Q, Lan R, He L, et al. A critical review of adsorption isotherm models for aqueous contaminants: curve characteristics, site energy distribution and common controversies. J Environ Manage. 2023;329:117104. doi: 10.1016/j.jenvman.2022.117104.

[62] Radke CJ, Prausnitz JM. Adsorption of organic solutes from dilute aqueous solution of activated carbon. Ind Eng Chem Fundam. 1972;11(4):445–451. doi: 10.1021/i160044a003.

[63] Yan H, Yang L, Yang Z, et al. Preparation of chitosan/poly(acrylic acid) magnetic composite microspheres and applications in the removal of copper(II) ions from aqueous solutions. J Hazard Mater. 2012;229–230:371–380. doi: 10.1016/j.jhazmat.2012.06.014.